Carbon 104 (2016) 253–259

Contents lists available at ScienceDirect

Carbon

journal homepage: www.elsevier.com/locate/carbon

Sulfur-mediated photochemical energy harvesting in nanoporous carbons

Alicia Gomis-Berenguer [a], Mykola Seredych [b], Jesus Iniesta [c], Joao C. Lima [d], Teresa J. Bandosz [b], Conchi O. Ania [a, *]

[a] ADPOR Group, Instituto Nacional del Carbon (INCAR, CSIC), 33011 Oviedo, Spain
[b] Department of Chemistry, City College of New York, New York, NY 10031, USA
[c] Institute of Electrochemistry, Faculty of Science, Univ. Alicante, 03080, Spain
[d] Univ. Nova de Lisboa, Lisboa, Portugal

ARTICLE INFO

Article history:
Received 8 December 2015
Received in revised form
3 February 2016
Accepted 1 March 2016
Available online 2 March 2016

ABSTRACT

This work provides new insights in the field of applied photochemistry based on semiconductor-free nanoporous carbons and its application to sunlight energy harvesting. Using carbon materials of increasing average pore size, chemical functionalization to introduce a variety of O- and S-containing functional groups and monochromatic light, we have shown the dependence of the photochemical conversion of phenol in the confinement of the carbons nanopore space with the wavelength of the irradiation source, the dimensions of the pore voids and their surface chemistry. The photochemical conversion of phenol inside the carbons pore space was found to be very sensitive to the nature of the S-containing groups and the confinement state of the adsorbed pollutant.

1. Introduction

The use of sunlight as a sustainable low cost source of energy remains a largely investigated topic due to its potential application in various fields [1,2]. After the first studies reporting the degradation of cyanides in solution upon irradiation of ZnO and TiO_2 electrodes [3–6], the interest in heterogeneous photocatalysis for the degradation of pollutants has significantly increased. However, advances in the area have rather been restricted to the use of inorganic semiconductors -mainly transition metal oxides and sulfides-that should be stable, nontoxic, inexpensive, as well as having suitable electronic band positions for an efficient visible light absorption.

An interesting approach to improve the usually low photonic efficiency of most photocatalysts is the incorporation of carbon additives; the strong carbon/semiconductor interfacial electronic effects and the high electron mobility in the carbon matrix boost the separation of photogenerated charge carriers, improving their possibility to react with electron donor/acceptors present in the medium [7–10].

More recently, the photochemical activity of nanoporous carbons has been reported, demonstrating their potential for an efficient use of light in chemical reactions in the confinement of pore spaces [11,12]. This has opened new perspectives for the application of carbon materials in photoluminescence and photocatalytic processes (ca. photooxidation of pollutants, regeneration of exhausted adsorbents, photoelectrochemical splitting of water and enhanced adsorption/oxidation) [13–19].

The conversion of light inside the carbon pore space has been found to be very sensitive to confinement effects and the surface functionalization of the carbon [20–22]. Several authors have reported the possibility to modulate the photochemical response and light absorption features of nanoporous carbons upon tuning the surface acidic/basic character and pore architectures. By introducing N and S-containing groups to the carbon and enhancing the interfacial molecule/carbon/light interactions (through adequate pore-guest matching), it is possible to favor the sunlight harvesting and its conversion into chemical reactions [22–26].

Aiming at understanding the mechanisms governing the conversion of light in chemical reactions in the pore space of nanoporous carbons, we herein report the combined effect of S-doping and nanopore size on the photooxidation of phenol. We show the dependence of the photochemical activity in the UV–visible range on the nature of the sulfur functionalities and pore dimensions,

* Corresponding author.
E-mail address: conchi.ania@incar.csic.es (C.O. Ania).

http://dx.doi.org/10.1016/j.carbon.2016.02.058

choosing the photooxidation of phenol as a model reaction.

2. Experimental

2.1. Materials

A series of nanoporous carbons with progressively changing pore structures were obtained from the activation of coal under CO_2 atmosphere (10 °C/min up to 850 °C in 100 mL/min N_2, then switch to CO_2, 10 mL/min) for variable periods of time. The samples were labelled as F, F1 and F4, where the number represents the increasing burn-off degree achieved in the activation. To introduce S-containing functional groups, F, F1 and F4 samples were exposed to H_2S (ca. 1000 ppm balanced in nitrogen, flow rate 150 mL/min) for 3 h at 800 °C (heating rate 10 °C/min). The nomenclature assigned to the S-doped carbons is the name of the initial material followed by "S" (i.e., F-S, F1-S and F4-S).

2.2. Irradiation set-up and phenol photooxidation

To isolate the effect of the carbon/light interactions taking place inside the pores, the photochemical reaction was carried out from the adsorbed state, irradiating aqueous suspensions of the nanoporous carbons loaded with the target pollutant [11,12]. The amount of phenol adsorbed in the pore system (ca. 90 μmol/g carbon) was below the maximum adsorption capacity of all carbons addressed in this work; this assures the confinement of phenol in the micropores [11,12], and prevents desorption during the irradiation (eliminating the contributions of direct photolysis and adsorption/desorption kinetics). Furthermore, the use of monochromatic light allows us to differentiate the conversion of high and low energy photons. Details on the phenol photooxidation procedure have been described elsewhere [12,20]. Briefly, suspensions of the carbon materials in a phenol solution are allowed to equilibrate until all phenol is completely removed, and then irradiated for 30 min under stirring. The solution is filtered out and analyzed. The carbons are further extracted with ethanol and the alcoholic solution is also analyzed (extraction yields are previously determined). Direct phenol photolysis was also performed for comparison. All the measurements were done at least in triplicate. A Xe lamp (300 W) coupled to a monochromator was used to irradiate the samples. The photon flux arriving at each wavelength was measured through ferrioxalate actinometry following IUPAC recommendations; experimental details are given in the Supplementary Information (SI), along with the corresponding values at each wavelength (Fig. S1).

2.3. Spin trapping electron spin resonance (ESR) measurements

The formation of paramagnetic species in solution during irradiation of the carbon suspensions was detected by a nitrone spin trapping agent (5-diethoxyphosphoryl-5-methyl-1-pyrroline-N-oxide, DEPMPO). This compound is capable of forming spin adducts with hydroxyl and superoxide radicals, creating more stable nitrone radicals that are easily detected by ESR spectroscopy in aqueous solution. About 0.5 g/L of the carbon samples were suspended in 5 mL of $HClO_4$ buffer (pH 3), and the appropriate volume of DEPMPO was added to the suspension to reach a final concentration of 18 mM. Samples were introduced in capillary quartz tubes and irradiated for 5, 10, 20 and 60 min (Philips TL K40W/05 lamp, with a broad emission peak centered at 365 nm). ESR spectra were immediately recorded from the solution (after filtering out the solids) at room temperature on a Bruker ESP 300E X band spectrometer with the following spectral parameters: receiver gain 105; modulation amplitude 0.52 G; modulation frequency 100 kHz, microwave frequency 9.69 GHz; microwave power 5.024 mW; conversion time 40.96 ms; center field 3450 G, sweep width 120 G. The intensity of the second line in the spectra was used for the quantification of the signals.

2.4. Textural characterization

The textural properties of the samples were determined by means of N_2 adsorption isotherms at −196 °C in a volumetric analyzer. Before the experiments, the samples were outgassed at 120 °C 17 h to constant vacuum (10^{-4} Torr). The specific surface area, S_{BET}, and pore volumes were evaluated from the gas adsorption isotherms using the Dubinin–Radushkevich equation. The pore size distribution in the full micro-/mesopore range was calculated from the N_2 adsorption isotherms using the 2D-NLDFT-HS (www.NLDFT.com) model assuming surface heterogeneity of carbon pores [27].

2.5. Elemental analysis

Samples were chemically characterized by elemental analysis. The determination of carbon, hydrogen and nitrogen was carried out by a LECO CHNS-932 (ASTM D-5373), sulfur was measured in a LECO S-144DR (ASTM D-4239) analyzer, while oxygen was directly measured in a LECO VTF-900 CHNS-932 microanalyzer. All the samples were previously dried under vacuum at 120 °C for 17 h.

2.6. Surface pH

The surface pH of the carbon samples was measured in an aqueous suspension containing 0.4 g of carbon sample powder added to 20 mL of distilled water. After equilibration under stirring overnight, the pH value was measured using a glass electrode.

3. Results and discussion

Fig. 1 (top) shows the photochemical conversion of phenol inside the confined nanopore space of carbons with gradually increasing pore size at selected wavelengths. The progressive activation of carbon F under CO_2 atmosphere to render samples F1 and F4 reflects in the evolution of porosity (in terms of surface area and pore volumes, see Table 1). The conversion values were normalized per photon flux to allow the comparison of the performance at different wavelengths (absolute conversion values are shown in Fig. S2). First of all, the phenol conversion in the nanoconfined state was higher than that of the photolytic reaction in a solution (photolysis is ca. 4% at 269 nm and negligible at longer wavelengths) for all carbons tested regardless the wavelength. This confirms the efficient use of light for the photooxidation of phenol in the constrained pore structure of the carbons, even at wavelengths corresponding to the visible range. Furthermore, the data shows interesting differences in the photochemical performance of the carbons at the different wavelengths, pointing out the outstanding role of porosity and surface functional groups.

As previously reported for other nanoporous carbons using various illumination conditions (i.e., monochromatic and polychromatic light and various irradiation set-up) [11,12,20,21], the dependence of the photochemical conversion on the wavelength followed a U-shaped pattern. For all the nanoporous carbons the conversion was more efficient at high (ca. 269 nm) and low (ca. 500 nm) energy photons corresponding to UV and visible light, respectively. Similarly, all carbons tested showed a minimum at 400 nm (Fig. 1), suggesting the presence of various photoactive sites in the carbons, which would be activated under different illumination conditions (incident photon energy).

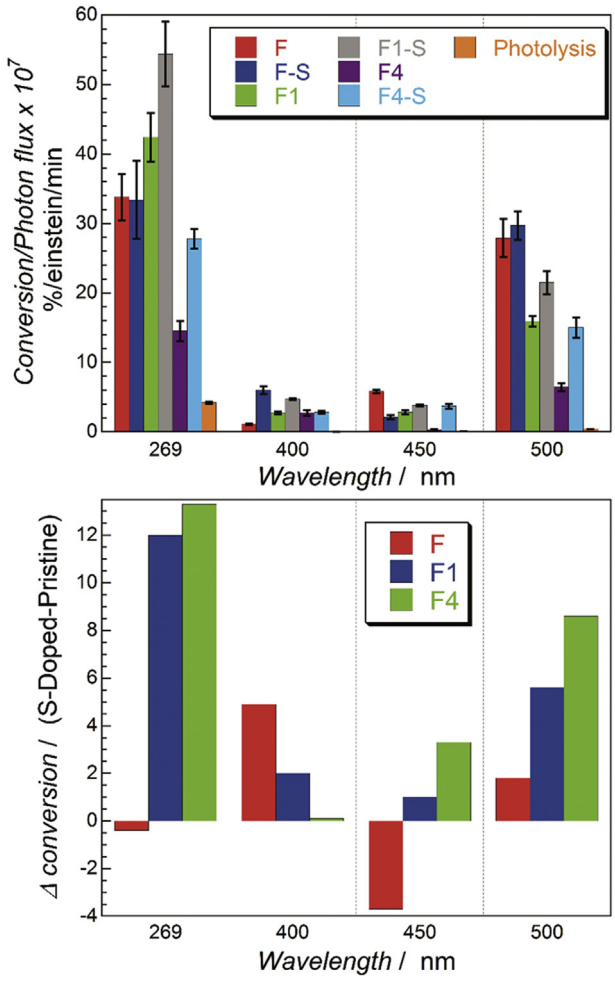

Fig. 1. (top) Normalized phenol conversion per incident flux at different wavelengths for the studied nanoporous carbons. (bottom) Effect of sulfur on the conversion of phenol, defined as the difference between the conversion in the S-doped and its corresponding as-received carbon. (A colour version of this figure can be viewed online.)

Table 1
Main textural parameters of the studied nanoporous carbons obtained from the equilibrium nitrogen adsorption isotherms at −196 °C.

	S_{BET} [$m^2\ g^{-1}$]	V_{PORES}[a] [$cm^3\ g^{-1}$]	Wo (DR)[b] [$cm^3\ g^{-1}$]	L[c] [nm]
F	800	0.35	0.34	0.93
F1	1150	0.50	0.55	1.37
F4	1800	0.84	0.80	2.00
F-S	765	0.32	0.32	0.85
F1-S	1090	0.49	0.41	1.04
F4-S	1535	0.75	0.56	1.52

[a] Total pore volume evaluated from the N_2 adsorption isotherms at −196 °C at p/p_0 ~0.99.
[b] Micropore volume evaluated from the Dubinin–Radushkevich method applied to N_2 adsorption isotherms.
[c] Mean narrow micropore size evaluated from the Stoeckli–Ballerini equation.

As for the effect of sulfur, the higher phenol conversions were obtained for the S-doped carbons at all the wavelengths, with respect to the pristine carbons. The exception is sample F, for which the performances of the as-received and S-doped carbons are quite similar. The superior photochemical conversion of the S-doped carbons was more pronounced at 269 and 500 nm, demonstrating the role of sulfur in the exploitation of both UV and visible light. This is more clearly seen in the difference in the conversion of the S-doped carbons vs. their corresponding undoped counterparts (Fig. 1, bottom). As shown, the effect of sulfur becomes more important for the carbons with a larger average pore size (samples F1 and F4); this could be partly attributed to the higher sulfur content in these carbons.

The enhanced effect of sulfur on the activity of nanoporous carbons was also reported for the photoelectrochemical water splitting using polychromatic light [22]; we herein correlate the conversion of another reaction (phenol photooxidation) with the wavelength of the irradiation source, the nanopore size and the nature of the sulfur groups.

The nanoporous carbons' features were modified by a gradual activation of carbon F under CO_2 atmosphere in order to obtain a series of materials with different average pore sizes. The progressive activation of the carbons is seen in the evolution of porous features (Table 1 and Fig. 2), whereas the chemical composition remained rather unchanged. The analysis of the textural changes was performed exclusively from the experimental N_2 adsorption isotherms at −196 °C; the use of CO_2 adsorption to analyze the narrow microporosity is not recommended in the case of highly functionalized carbons (O-and S-doped) due to the occurrence of specific interactions with the surface groups [28,29].

As expected, the gradual activation caused an increase in the N_2 uptake (Fig. 2) due to the creation of pores and their enlargement. The pristine carbon showed a type Ia adsorption isotherm [30], characteristic of highly microporous materials with a narrow distribution of micropores pore sizes (w < 1 nm), whereas the activation caused an opening of the knee of the N_2 isotherm (type IIb shape) characteristic of materials with wider micropores and narrow mesopores (w < 2.5 nm). This is seen in the PSD calculated from the N_2 adsorption isotherms (Fig. 2). It is noted that the S-doped carbons have a lower porosity that their corresponding non-doped counterparts (there is a slight drop in the surface area and pore volumes after the incorporation of sulfur). In contrast, the changes in the PSD seen in the full micro/mesopore range are subtle (Fig. 2), affecting mostly the larger pores. Indeed, a slight narrowing of the average pore size (evidenced by the L parameter, Table 1) was observed, indicating that sulfur is mainly incorporated in the larger pores. This effect is more noticeable for sample F4-S that presents the highest burn-off degree and the largest amount of sulfur. Similar findings have been reported for the sulfurization of charcoals [31].

The amount of sulfur incorporated depends on the porosity of the carbons, being almost twice larger for the most activated carbon compared to the pristine F sample. The oxygen content in the initial carbon is rather small (Table 2), and did not increase much after the sulfur doping, suggesting that most of sulfur is in the form of sulfides, thiophenes, and disulfides (non-oxidized groups). The increase in the oxygen content after the incorporation of sulfur was more pronounced for the carbons with wider pores, pointing to the presence of oxidized sulfur groups. To evaluate the dependence of the photochemical activity of the carbons on the amount and nature of the sulfur species, the chemistry of the S-groups was investigated by XPS (Table 2, Tables S1-S3 and Fig. S3-S5 in SI) and TPD-MS (Fig. 3 and Fig. S6).

XPS analysis of the S 2*p* core level spectra revealed the presence of two peaks at 163.6 and 164.7 eV (Fig. S4) that can be assigned to thiophenes and disulfide groups, and oxidized sulfur in thioethers, respectively [32]. No signal corresponding to free elemental sulfur was detected. Interestingly, there is a clear correlation on the relative distribution of the sulfur peaks with the burn off degree of the carbons, as the intensity of the peak located at lower binding energies (i.e., non-oxidized sulfur) decreases with the activation

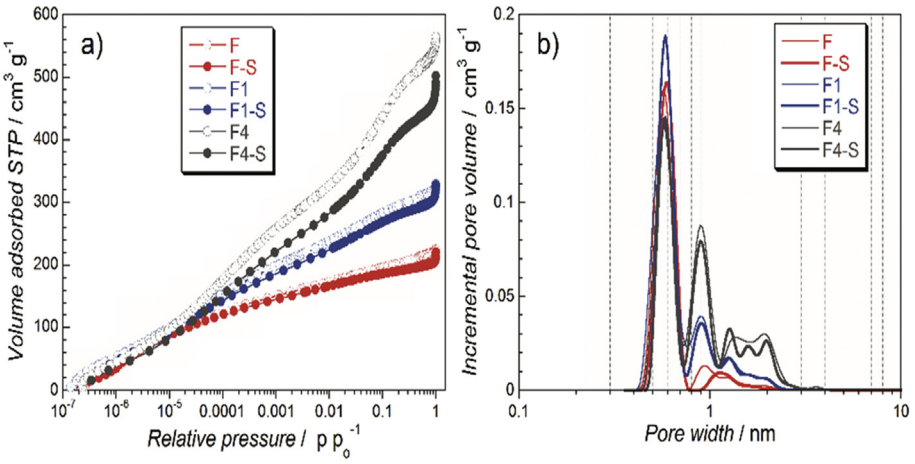

Fig. 2. (a) Nitrogen adsorption isotherms measured at −196 °C of the studied carbons and (b) pore size distributions obtained applying the 2D-NLDFT-HS method to the N_2 data. (A colour version of this figure can be viewed online.)

Table 2
Chemical composition obtained by elemental analysis (wt.%), surface elements determined by XPS (at.%) and surface pH.

Sample	Elemental analysis, wt. %				XPS analysis, at. %				Surface pH
	C	H	O	S	C	O	S	O/C	
F	96.15	0.70	2.90	0.11	87.4	12.6	ND	0.14	8.1
F1	95.92	0.45	3.43	0.10	90.2	9.8	ND	0.11	8.2
F4	95.85	0.22	3.73	0.11	91.4	8.6	ND	0.10	8.0
F-S	92.31	0.46	3.62	3.62	91.4	6.1	2.5	0.07	7.9
F1-S	88.23	0.37	6.07	5.34	87.7	10.5	1.8	0.12	7.6
F4-S	87.29	0.25	5.54	6.93	84.0	14.6	1.4	0.17	7.4

ND – non detected.

the XPS analysis. In fact, according to literature [31], sulfur–carbon complexes in thiol and sulfide configurations are very reactive and can be easily oxidized (chemisorbed oxygen or released from the decomposition of O-groups) into SO and SO_2 evolving groups upon heating during the TPD assays. Thus, the detection of SO and SO_2 cannot be used as a definitive confirmation of the chemical state of the sulfur bonded to the carbon surface.

To clarify this, we performed a deconvolution of the *m/z* thermal profiles; as both *m/z* 48 and 64 signals showed similar trends (Fig. S6), we further discuss those of *m/z* 48. Data corresponding to the devolution analysis of the S-doped carbons is shown in Fig. 4.

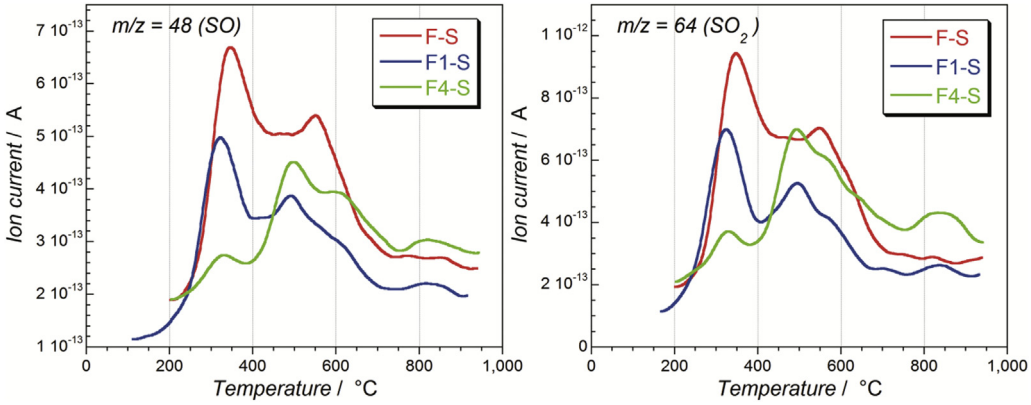

Fig. 3. Profiles from the temperature programmed desorption corresponding to *m/z* 48 and 64 signals for the studied carbons. (A colour version of this figure can be viewed online.)

treatment of the carbons, as a result of surface oxidation. As the overall sulfur content also increased with the activation, this suggests that the formation of oxidized sulfur groups is favored in carbons with larger pore sizes. This is expected to affect the photochemical activity of the carbons, as discussed below.

TPD-MS also revealed interesting features of the S-containing groups in the carbons. Besides the *m/z* signals corresponding to CO and CO_2 evolution -upon decomposition of O-containing groups as quinones and carboxylic acids-, only those corresponding to the release of SO (*m/z* 48) and SO_2 (*m/z* 64) were detected (Fig. 3). This would indicate that all released sulfur is bonded to the carbon surface in oxidized configurations, which apparently contradicts

There are three main peaks in the profiles that can be assigned to thiol groups (P1 at ca. 330 °C), and to the decomposition of oxidized sulfides (P2 and P3 at ca. 500 and 600 °C, respectively) [33,34]. The contribution of P1 is quite high for the carbon with the narrowest pore size (sample F-S), and it gradually decreases with an increased activation level, while the relative abundances of P2 and P3 became larger. This corroborates that above 500 °C, the *m/z* 48 and 64 signals are partly attributed to the presence of sulfur in an oxidized form, in agreement with the XPS data. This supports our hypothesis that the incorporation of oxidized sulfur groups to the carbon surface is favored in the carbons with large pores, whereas thiols and/or disulfides are dominant for the carbon with narrow pore

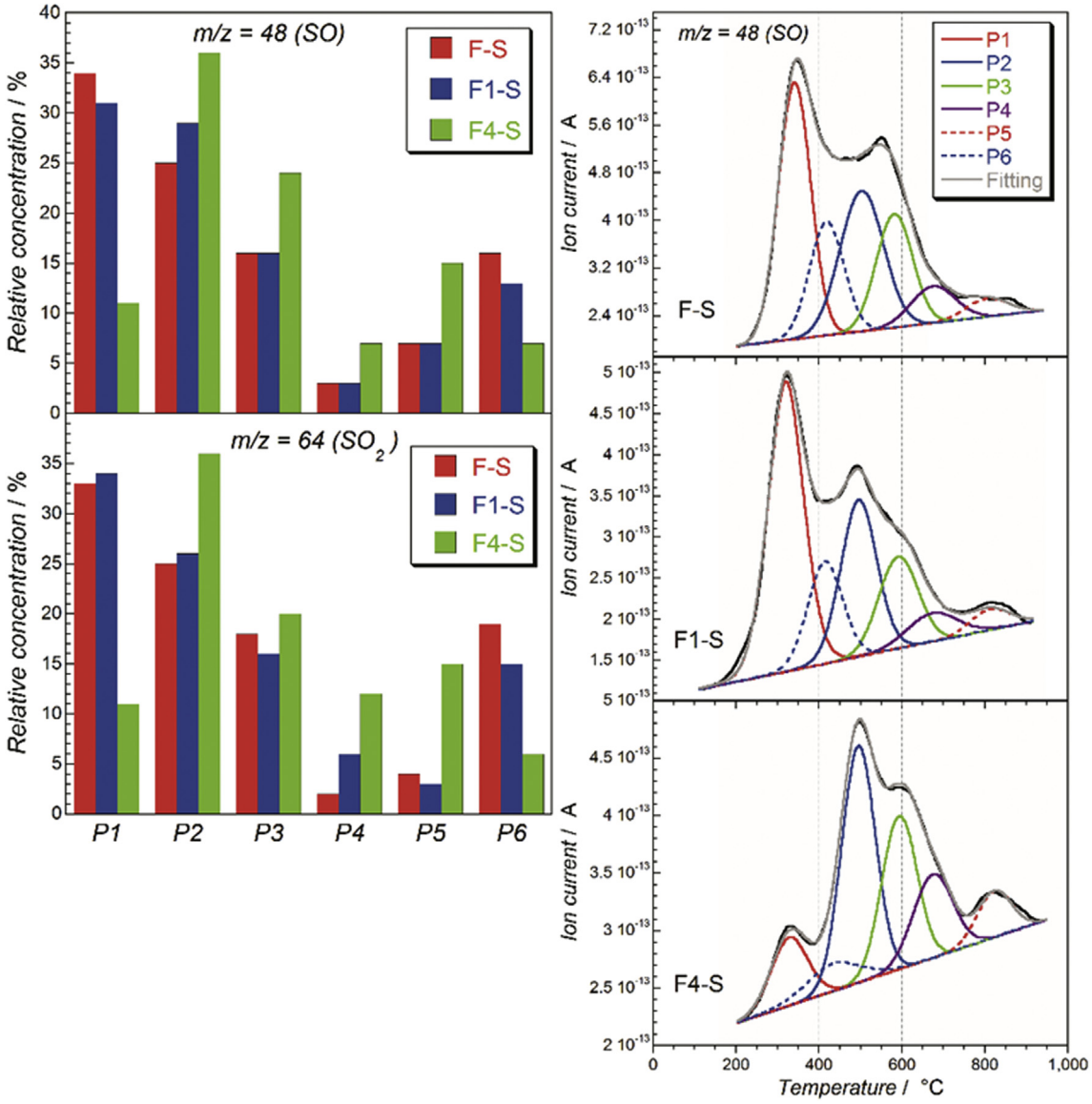

Fig. 4. Deconvolution of TPD-MS profiles corresponding to *m*/*z* 48 on the S-doped nanoporous carbons, and relative abundance of the deconvoluted peaks of SO (*m*/*z* 48) and SO_2 (*m*/*z* 64). (A colour version of this figure can be viewed online.)

sizes. In fact, in pores with sizes of the fraction of nanometers only sulfur incorporated to aromatic rings in thiophenic configurations can exist, owing to spatial constraints for bulky sulfoxides or sulfones.

Taking all of these into account, the differences in the photochemical response observed on the carbons must be discussed in terms of their differences in surface chemistry and the confinement state of phenol in the nanopore space. The light absorption features of amorphous carbons depend on the electronic transitions involving the sp^2 carbon clusters [35–39] and/or the activation of chromophoric groups on the carbon surface [21–24]. Upon irradiation of the carbon excitons (holes or electrons) are formed, and if their recombination is delayed they can participate in charge transfer reactions with electron donors. Medium to low range excitons (Frenkel-like created in the π-π^* and σ-π electronic transitions involving zig-zag and carbine-like sites [38,40]) are expected to be dominant in all nanoporous carbons [20,40–42]. Charge-transfer excitons formed by localized states involving O-, S- and C- atoms may be formed in F1 and F4 samples as well as in the S-doped carbons, although they are expected to be negligible in the initial F carbon (due to its lower level of functionalization).

For the undoped carbons, the gradual activation is not expected to produce changes in their optical response since it affects the pore size (i.e., enlargement), with no significant changes in surface chemistry or the sp^2/sp^3 hybridization of carbon atoms. The lower conversions for F1 and F4 -compared to that for F carbon-are then attributed to the weaker adsorption of phenol molecules in the large pores, thus decreasing the probability of splitting of the photogenerated exciton by a fast charge transfer with electron donors and/or holes scavengers (i.e., oxygen, adsorbed phenol, water molecules to form radicals) [20,21].

In the case of the S-doped carbons several scenarios are plausible. First, the incorporation of sulfur provokes a narrowing of the average pore size (Table 1); this would boost the separation of the photogenerated charge carriers (holes and electrons) in the nanopores due to the proximity of the adsorbed phenol molecules

[20,21]. The fast charge transfer is favored in the S-doped carbons, as the presence of heteroatoms lowers the energy difference between the electronic levels of the carbons [43,44]. The stabilization of the holes through the oxidation of water (coadsorbed in the nanopores) to form reactive oxygen species in the S-doped carbons was supported by spin resonance spectroscopy using a nitrone as trapping chemical [44]. A quantification of the radical species detected in the pristine carbons compared to the S-doped carbons is shown in Fig. 5 (the corresponding EPR spectra of all the samples are compiled in Fig. S8).

The electrons generated are delocalized/spread through the sp^2 domains of the carbons, allowing their participation in some other electronic transitions with acceptors present in the medium (i.e., oxygen, transfer to the chromophores). Additionally, the S- and O-containing groups can act as chromophores [45–47], photogenerating excitons that also participate in the observed photochemical reactions. Various oxidized forms of sulfur (thioesters and sulfones) and O-containing groups have been reported to act as chromophores [45,47]. Oxidized sulfur groups are bulky moieties located in the wide micropores of the carbons, at the edges of the aromatic graphitic sheets. The conjugation with the sp^2 network of the basal planes of the carbons favors the separation of the charge carriers upon irradiation. The different chemical environments of the S-groups explain the trend observed in the photochemical response of the carbons. As seen from Fig. 1, the incorporation of sulfur to the initial carbon improved the conversion of phenol but the effect was less pronounced than that on the activated counterparts. This suggests that thiols and/or sulfides -the dominant moieties in FS- do not exhibit photoactivity towards oxidation at the studied wavelengths. In contrast, when sulfur is predominantly in oxidized forms, the photooxidative activity of the carbons is largely improved, particularly at 269 and 500 nm and for sample F4-S, which showed an abundance of these groups (Fig. 3). This indicates the specific role of S and O containing groups in the oxidation of phenol.

4. Conclusions

We show the pronounced effect of a confinement, wavelength and S-functionalization on the exploitation of the energy harvesting performance of nanoporous carbons. When sulfur is incorporated to a carbon matrix the conversion of light into a chemical reaction (i.e., photooxidation of phenol, generation of O-radicals) becomes more efficient compared to that on the undoped carbons. An adequate pore architecture is also essential to obtain higher conversions in the constrained pore space; adjusting the pore size to the dimensions of the adsorbed molecule inhibits the recombination of the photogenerated excitons, facilitating the stabilization of the holes and electrons through the reaction with electron donors and/or holes scavengers (i.e., dissolved oxygen, adsorbed phenol, water molecules to form radicals). In all cases conversion in the confined pore space of the functionalized carbons were higher than those in a solution.

Besides S-doping, the light-stimulated conversion of phenol was very sensitive to the nature of the sulfur moieties incorporated to the carbon matrix, as well as highly dependent on the wavelength of the irradiation source. This behavior is also linked to the ability of the oxidized sulfur moieties to act as chromophores, being activated by low energy photons (sunlight). This was corroborated by the higher amount of oxygen radical species measured in the S-doped carbons. The versatility of nanoporous carbons in terms of structure, porosity and surface chemistry makes it very promising to invest on their use as sustainable photoactive materials for various applications (e.g. photoelectrochemical water splitting for hydrogen and oxygen evolution, pollutants photooxidation). The challenge, however still remains in boosting their sunlight energy harvesting ability by balancing the surface composition, porosity, and charge-carrier mobility.

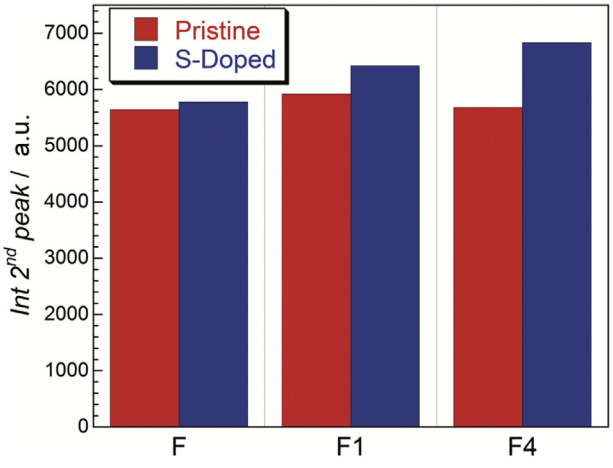

Fig. 5. Quantification of the oxygen radical species detected from the signal corresponding to DEPMPO-OH adducts by integration of the ESR profiles. (A colour version of this figure can be viewed online.)

Acknowledgments

COA thanks the financial support of the European Research Council through a Consolidator Grant (ERC-CoG-648161-PHOROSOL) and the Spanish MINECO (CTM2014/56770-R). AGB thanks her PhD fellowship (BES-2012-060410). TJB acknowledges the NSF support (CBET 1133112).

Appendix A. Supplementary data

Supplementary data related to this article can be found at http://dx.doi.org/10.1016/j.carbon.2016.02.058.

References

[1] E. Pelizzetti, N. Serpone, in: Photocatalysis: Fundamentals and Applications, Wiley, New York, 1989.
[2] M.R. Hoffmann, S.T. Martin, W. Choi, D.W. Bahnemann, Environmental applications of semiconductor photocatalysis, Chem. Rev. 95 (1995) 69–96.
[3] T.I. Barry, F.S. Stone, The reactions of oxygen at dark and irradiated zinc oxide surface, Proc. R. Soc. 255 (1960) 124–144.
[4] F. Romero-Rossi, F.S. Stone, in: 2nd Intern. Congr. On Catalysis, Paris, 1960, p. 1481.
[5] R.I. Bickley, G. Munuera, F.S. Stone, Photoadsorption and photocatalysis at rutile surfaces. 2. Photocatalyitic oxidation of isopropanol, J. Catal. 31 (1973) 398–407.
[6] A. Fujishima, K. Honda, Electrochemical photolysis of water at a semiconductor electrode, Nature 238 (1972) 37–38.
[7] J. Matos, J. Laine, J.M. Herrmann, Synergy effect in the photocatalytic degradation of phenol on a suspended mixture of Titania and activated carbon, Appl. Catal. B Environ. 8 (1998) 281–291.
[8] R. Leary, A. Westwood, Carbonaceous nanomaterials for the enhancement TiO_2 photocatalysis, Carbon 49 (2011) 741–772.
[9] J.L. Faria, W. Wang, Ch 13, in: P. Serp, J.L. Figueiredo (Eds.), Carbon Materials for Catalysis, John Wiley & Sons, New York, 2009, pp. 481–506.
[10] C.O. Ania, L.F. Velasco, T. Valdes-Solis, Ch 17, in: J.M.D. Tascon (Ed.), Novel Carbon Adsorbents, Elsevier, London, 2012, p. 521.
[11] L.F. Velasco, J.C. Lima, C.O. Ania, Visible-light photochemical activity of nanoporous carbons under monochromatic light, Angew. Chem. 53 (2014) 4146–4148.
[12] L.F. Velasco, I.M. Fonseca, J.B. Parra, J.C. Lima, C.O. Ania, Photochemical response of activated carbons under UV irradiation, Carbon 50 (2012) 249–258.
[13] L. Bao, Z.L. Zhang, Z.Q. Tian, L. Zhang, C. Liu, Y. Lin, B. Qi, D.W. Pang, Electrochemical tuning luminescent carbon nanodots: from preparation to luminescence mechanism, Adv. Mater 23 (2011) 5801–5806.

[14] Q. Bao, J. Zhang, C. Pan, J. Li, C.M. Li, J. Zang, D.Y. Tang, Recoverable photoluminescence of flame-synthesized multiwalled carbon nanotubes and its intensity enhancement at 240 K, J. Phys. Chem. C 111 (2007) 10347–10352.
[15] T.J. Bandosz, E. Rodriguez-Castellon, J.M. Montenegro, M. Seredych, Photoluminescence of nanoporous carbons: opening a new application route for old materials, Carbon 77 (2014) 651–659.
[16] M. Seredych, O. Mabayoje, T.J. Bandosz, Visible-light-enhanced interactions of hydrogen sulfide with composites of Zinc (Oxy)hydroxide with graphite oxide and graphene, Langmuir 28 (2012) 1337–1346.
[17] D. Pan, J. Zhang, Z. Li, M. Wu, Hydrothermal route for cutting graphene sheets into blue-luminiscent graphene quantum dots, Adv. Mater 22 (2010) 734–738.
[18] I. Velo-Gala, J.J. Lopez-Peñalver, M. Sanchez-Polo, J. Ribera-Utrilla, Activated carbon as photocatalyst of reactions in aqueous phase, Appl. Catal. B 142 (2013) 694–704.
[19] R. Ocampo-Pérez, M. Sánchez-Polo, J. Rivera-Utrilla, R. Leyva-Ramos, Enhancement of the catalytic activity of TiO_2 by using activated carbon in the photocatalytic degradation of cytarabine, Appl. Catal. B Environ. 104 (2011) 177–184.
[20] L.F. Velasco, A. Gomis-Berenguer, J.C. Lima, C.O. Ania, Tuning the surface chemistry of nanoporous carbons for enhanced nanoconfined photochemical activity, Chem. Cat. Chem. 7 (2015) 3012–3019.
[21] A. Gomis-Berenguer, J. Iniesta, V. Maurino, J.C. Lima, C.O. Ania, Boosting visible light conversion in the confined pore space of nanoporous carbons, Carbon 96 (2016) 98–104.
[22] C.O. Ania, M. Seredych, E. Rodriguez-Castellon, T.J. Bandosz, Visible light driven photoelectrochemical water splitting on metal free nanoporous carbon promoted by chromophoric functional groups, Carbon 79 (2014) 432–441.
[23] M. Seredych, L. Messali, T.J. Bandosz, Analysis of factors affecting visible and UV enhanced oxidation of dibenzothiophenes on sulfur-doped activated carbons, Carbon 62 (2013) 356–364.
[24] T.J. Bandosz, J. Matos, M. Seredych, S.Z. Islam, R. Alfano, Photoactivity of S-doped nanoporous activated carbons: a new perspective for harvesting solar energy on carbon-based semiconductors, Appl. Catal. A 445 (2012) 159–165.
[25] D. Pan, J. Zhang, Z. Li, M. Wu, Hydrothermal route for cutting graphene sheets into blue-luminescent graphene quantum dots, Adv. Mater 22 (2010) 734–738.
[26] M. Seredych, T.J. Bandosz, Effect of the graphene phase presence in nanoporous S-doped carbon on photoactivity in UV and visible light, Appl. Catal. B 147 (2014) 842–850.
[27] J. Jagiello, J.P. Olivier, Carbon slit pore model incorporating surface energetical heterogeneity and geometrical corrugation, Adsorption 19 (2013) 777–783.
[28] M. Seredych, J. Jagiello, T.J. Bandosz, Complexity of CO2 adsorption on nanoporous sulfur-doped carbons—is surface chemistry an important factor? Carbon 74 (2014) 207–217.
[29] T.J. Bandosz, M. Seredych, E. Rodríguez-Castellón, Y. Cheng, L.L. Daemen, A.J. Ramírez-Cuesta, Carbon 96 (2016) 856.
[30] M. Thommes, K. Kaneko, A.V. Neimark, J.P. Olivier, F. Rodriguez-Reinoso, J. Rouquerol, K.S.W. Sing, Physisorption of gases, with special reference to the evaluation of surface area and pore size distribution (IUPAC Technical Report), Pure Appl. Chem. 87 (2015) 1051–1069.
[31] B.R. Puri, R.S. Hazra, Carbon-sulphur surface complexes on charcoal, Carbon 9 (1971) 123–134.
[32] J.F. Moulder, W.F. Stickle, P.E. Sobol, K.D. Bomben, in: Standard Spectra for Identification and Interpretation of XPS Data, Perkin Elmer, Eden Prairie, MN, 1992.
[33] A.P. Terzyk, Further insights into the role of carbon surface functionalities in the mechanism of phenol adsorption, J. Colloid Interf. Sci. 268 (2003) 301–329.
[34] W. Feng, S. Kwon, X. Feng, E. Borguet, R.D. Vidic, Sulfur impregnation on activated carbon fibers through H_2S oxidation for vapor phase mercury removal, J. Env. Eng. 132 (2006) 292–300.
[35] A.D. Modestov, J. Gun, O. Lev, Graphite photoelectrochemistry study of glassy carbon, carbon-fiber and carbon-black electrodes in aqueous electrolytes by photocurrent response, Surf. Sci. 417 (1998) 311–322.
[36] J. Robertson, Mechanical properties and coordinations of amorphous carbons, J. Phys. Rev. Lett. 68 (1992) 220–223.
[37] C. Oppedisano, A. Tagliaferro, Relationship between sp(2) carbon content and E-04 optical gap in amorphous carbon-based materials, Appl. Phys. Lett. 75 (1999) 3650–3652.
[38] L.R. Radovic, B. Bockrath, On the chemical nature of graphene edges: origin of stability and potential for magnetism in carbon materials, J. Am. Chem. Soc. 127 (2005) 5917–5927.
[39] Y. Zhu, X. Li, Q. Cai, Z. Sun, G. Casillas, M.J. Yacaman, R. Verduzco, J.M. Tour, Quantitative analysis of structure and bandgap changes in graphene oxide nanoribbons during thermal annealing, J. Am. Chem. Soc. 134 (2012) 11774–11780.
[40] D. Lee, J. Seo, X. Zhu, J. Lee, H.-J. Shin, J.M. Cole, T. Shin, J. Lee, H. Lee, H. Su, Quantum confinement-induced tunable exciton states in graphene oxide, Sci. Rep. 3 (2013) 2250.
[41] X. Zhu, H. Su, Exciton characteristics in graphene epoxide, ACS Nano 8 (2014) 1284.
[42] G. Xie, K. Zhang, B. Guo, Q. Liu, L. Fang, J.R. Gong, Graphene-based materials for hydrogen generation from light-driven water splitting, Adv. Mater 25 (2013) 3820–3839.
[43] V.V. Strelko, V.S. Kuts, P.A. Thrower, On the mechanism of possible influence of heteroatoms of nitrogen, boron and phosphorous in a carbon matrix on the catalytic activity of carbons in electron transfer reactions, Carbon 38 (2000) 1499–1524.
[44] H. Karoui, F. Chalier, J.-P. Fineta, P. Tordo, DEMPO: an efficient tool for the coupled ESR-spin trapping of alkylperoxyl radicals in water, Org. Biomol.Chem. 9 (2011) 2473–2480.
[45] J.E. Beecher, T. Durst, J.M.J. Fréchet, A. Godt, A. Pangborn, D.R. Robello, C.S. Willand, D.J. Williams, New chromophores containing sulfonamide, sulfonate, or sulfoximide groups for second harmonic generation, Adv. Mater 5 (1993) 632–634.
[46] G. Jin, Y. Zhang, W. Cheng, Poly(p-aminobenzene sulfonic acid)-modified glassy carbon electrode for simultaneous detection of dopamine and ascorbic acid, Sens. Act. B 107 (2005) 528–534.
[47] M. Baca, G.E. Borgstahl, M. Boissinot, P.M. Burke, D.R. Williams, K.A. Slater, E.D. Getzoff, Complete chemical structure of photoactive yellow protein: novel thioester-linked 4- hydroxycinnamyl chromophore and photocycle chemistry, Biochemistry 33 (1994) 14369–14377.